Author Manuscript

Author Manuscript

Author Manuscript

Author Manuscript

HHS Public Access

Author manuscript

Nat Neurosci. Author manuscript; available in PMC 2022 February 18.

Published in final edited form as:

Nat Neurosci. 2019 November ; 22(11): 1883–1891. doi:10.1038/s41593-019-0494-0.

Widespread temporal coding of cognitive control in human prefrontal cortex

Elliot H. Smith[1,•], **Guillermo Horga**[2,•], **Mark J. Yates**[3], **Charles B. Mikell**[4], **Garrett P. Banks**[3], **Yagna J. Pathak**[3], **Catherine A. Schevon**[5], **Guy M. McKhann II**[3], **Benjamin Y. Hayden**[6], **Matthew M. Botvinick**[7], **Sameer A. Sheth**[8,*]

[1.]Department of Neurosurgery, University of Utah, Salt Lake City, UT, 84132, USA

[2.]New York State Psychiatric Institute, New York, NY, 10032, USA

[3.]Department of Neurological Surgery, Columbia University Medical Center, New York, NY, 10032, USA

[4.]Department of Neurosurgery, Stony Brook University, Stony Brook, NY, 11794, USA

[5.]Department of Neurology, Columbia University Medical Center, New York, NY, 10032, USA

[6.]Department of Neuroscience, University of Minnesota, Minneapolis, MN, USA

[7.]DeepMind, London N1C 4AG, UK.

[8.]Department of Neurosurgery, Baylor College of Medicine, Houston, TX 77030

Abstract

When making decisions we often face the need to adjudicate between conflicting strategies or courses of action. Our ability to understand the neuronal processes underlying conflict processing is limited on the one hand by the spatiotemporal resolution of fMRI and, on the other, by imperfect cross-species homologies in animal model systems. Here we examine responses of single neurons and local field potentials in human neurosurgical patients in two prefrontal regions critical to controlled decision-making, dorsal anterior cingulate cortex (dACC) and dorsolateral prefrontal cortex (dlPFC). While we observe typical modest conflict related firing rate effects, we find a widespread effect of conflict on spike-phase coupling in dACC and on driving spike-field coherence in dlPFC. These results support the hypothesis that a cross-areal rhythmic neuronal

Users may view, print, copy, and download text and data-mine the content in such documents, for the purposes of academic research, subject always to the full Conditions of use:http://www.nature.com/authors/editorial_policies/license.html#terms

[*]corresponding author: Sameer.Sheth@bcm.edu.

Author Contributions

S.A.S., C.B.M., M.J.Y., and E.H.S. designed the experiments. E.H.S., C.B.M., M.J.Y., Y.J.P., C.A.S., G.M.M. and S.A.S were involved with collecting the data. E.H.S., G.P.B., and G.H. analyzed the data. E.H.S., S.A.S., G.H., B.Y.H., M.M.B., and M.J.Y., wrote the manuscript. All authors provided edits to the manuscript.

[•]indicates equal contribution

Competing Interests

The authors declare no competing interests.

Data Availability Statement

Data are available from the authors upon reasonable request and with permission of the Columbia University Medical Center Institutional Review Board.

Author Manuscript Author Manuscript Author Manuscript Author Manuscript

coordination is intrinsic to cognitive control in response to conflict, and provide new evidence to support the hypothesis that conflict processing involves modulation of dlPFC by dACC.

Introduction

As we navigate through our daily lives, we are often confronted with choices involving competing or conflicting potential courses of action[1]. To resolve this *cognitive conflict*, we must summon additional cognitive resources – that is, we must both *monitor* and *resolve* the conflict. For example, imagine driving through a busy downtown and seeing the next traffic light turn green – normally a signal to go – but a slow pedestrian is in the crosswalk. To make the optimal decision, the driver must conjure additional cognitive resources to assess the pedestrian's speed, estimate the trajectory of the car, and determine whether other cars are following closely behind, to decide whether braking or swerving would be optimal. This capacity to monitor conflict and implement control is a vital, yet poorly understood, element of the repertoire of flexible intelligent organisms[2,3]. Understanding its mechanisms is essential for developing treatments for neuropsychiatric disorders associated with impaired conflict processing, and, since conflict is a useful model for other types of executive control, of control in general[4].

A good deal of research implicates the dorsal prefrontal cortex, especially the dorsal anterior cingulate cortex (dACC) and dorsolateral prefrontal cortex (dlPFC), in the monitoring and resolution of cognitive conflict[5]. For example, a wealth of imaging and electrophysiology data from humans and non-human animals supports the hypothesis that these regions play a critical role in one or both processes[6–13]. Moreover, lesions to these regions lead to a variety of impairments in control functions[14]. Prominent computational and theoretical models ascribe to these regions several features that are critical to a control process: monitoring goal-relevant variables, evaluating relative costs and benefits of choice alternatives, maintaining rule sets and goal-related information in working memory, and producing adaptive biases towards more successful behavior[3,15–18]. This work dovetails with careful computational studies for how systems with limited cognitive capacity can trade off between multiple competing sources of guidance[18,19]. That work in turn results in specific circuit-level predictions for how cognitive control, in response to conflict, can be implemented. In particular, it suggests that dACC serves as a conflict monitor and that dlPFC, located downstream of dACC, serves to implement conflict-related changes[2,3,20]. The idea that these two regions are both involved in conflict processing but have distinct roles has proven difficult to test given the paucity of studies that directly compare the activities of these two regions using neuron-level recording methods.

On one hand, human neuroimaging studies find clear correlates of conflict, but lack the temporal resolution to identify circuit-level correlates[21]. On the other, primate neurophysiology studies, which have high temporal and spatial resolution, have generally failed to find clear correlates of cognitive conflict[13,22]. Rodents do not have a clear homologue of either dACC or dlPFC, making interpretation of their data challenging[23,24]. The reasons for the disconnect between non-human primate electrode recording studies and human neuroimaging are not clear. One reason may be that animal studies require

Author Manuscript Author Manuscript Author Manuscript Author Manuscript

a very large number of trials; the resulting overtraining may systematically alter conflict processing[25,26]. Another likely factor is that fMRI and single unit activity do not have a clear one-to-one mapping, so there may be other features of the brain responses that predict conflict other than average firing rate responses.

Control, like many other aspects of executive function, requires coordination of activity across regions. This fact motivates the hypothesis that the major signatures of control would be observed in relation to the local field potential (LFP), which is thought to provide a mechanism for coordination across multiple brain structures[27]. LFP is distinct from unit activity and appears to be a better predictor of hemodynamic responses than average unit firing in some cases[28,29]. Furthermore, an extensive EEG literature provides reason to believe that oscillations contain information critically related to conflict processing. For example, variations in theta (4–8 Hz) range oscillations over frontal EEG contacts, known as frontal midline theta, have been repeatedly shown to reflect conflict and error processing, attentional control, and reinforcement-learning signals[30,31]. Such findings have been extended and refined with the few existing studies using human intracranial EEG[32,33]. This literature has led to an increasing number of theories positing a fundamental role for oscillatory activity in decision-making and cognition more generally[3,34]. An increasingly substantial body of evidence has been demonstrating the importance of neuronal spiking activity as it relates to the background LFP. This alignment of spiking with LFPs, or spike-field coherence (SFC), has proven to be a potent channel for coordination of neuronal populations, both locally and across brain regions[35]. For these reasons, our analyses focused on the spike-field coherence within dACC and dlPFC.

Here we examined simultaneously collected single neuron responses and LFPs in dACC and dlPFC in human neurosurgical patients. We found modest neuronal firing rate correlates of conflict in dACC and negligible ones in dlPFC. On the other hand, we found robust effects of conflict on the preferred phase of spiking in dACC (but not in dlPFC), but greater conflict-related spike-field coherence changes in dlPFC (than in dACC). These results support the hypothesis that processing cognitive conflict requires cross-areal coordination mediated at least in part by oscillatory activity. Moreover, they are consistent with the hypothesis that conflict processing involves monitoring by dACC and control by dlPFC[20]. Finally, our results show how neural codes that combine information in the spiking and oscillatory frequency (LFP) domains can facilitate the types of coordinated computation needed for executive control and provide important constraints on computational models of conflict processing.

Results

Limited, mixed firing rate code for conflict in dACC

We simultaneously recorded firing rates of single neurons in dACC, and LFPs in both dACC and dlPFC, in 6 human patients with medically refractory epilepsy undergoing intracranial recordings to detect seizures (Figure 1a; Supplementary Tables 1,2, and 3). Subjects performed the multi-source interference task (MSIT), a task that independently manipulates both spatial (Simon) and flanker (Eriksen) types of decision conflict (Figure 1b). Subjects had an overall low error rate (average of 1.4 ± 2.7% per session) and exhibited

Author Manuscript Author Manuscript Author Manuscript Author Manuscript

the hallmark behavioral signature of tasks demanding cognitive control: increasing reaction time (RT) with increasing level of decision conflict (Figure 1c).

We recorded firing rates from 136 well-isolated dACC neurons (Figure 2a). To classify neurons based on firing rate coding of task-relevant variables, we used a sliding-window generalized linear model (GLM) incorporating three factors corresponding to the three main task variables: decision conflict, response identity, and feedback-valence. We defined decision conflict as the sum of the two binary variables corresponding to the two forms of conflict. We focused our analysis on the period of time after cue presentation and before the behavioral response. We thus chose a time window 250–750 ms after cue presentation for the subsequent analyses. In our sample, 10.3% of dACC neurons (n = 14/136) were selective for decision conflict (Figure 2b), 8.8% (n = 12/136) were selective for response identity (Supplementary Figure 1a), and 8.1% (n = 11/136) were selective for feedback valence (Supplementary Figure 1b). We saw very little overlap among the different neuron classes, suggesting that these forms of conflict are encoded in largely disjoint sets of cells (Figure 2c). The majority of dACC neurons recorded (72.8%, n = 99/136) did not exhibit selectivity for any of the task variables based on firing rate. Nonetheless, it is clear that some human dACC neurons do employ a detectable firing rate coding scheme for task-relevant features, although these neurons are relatively uncommon.

Temporal code for decision conflict in dACC

We next tested the hypothesis that PFC neurons employ a temporal-coding strategy in the context of controlled decision-making. Of the three main task features, we focused our analysis on decision conflict, as this was the primary task manipulation (analyses of other features are presented in Supplementary Figure 2). Specifically, we hypothesized that temporal patterns of neuronal spiking relate to population oscillatory activity, and that this relationship is modulated in a conflict-level-dependent fashion.

We measured SFC for each neuron in relation to the LFP in dACC. We observed significant increases in SFC in the beta and theta ranges. These findings indicate that dACC spike timing could be predicted from population-level oscillations in these two frequency ranges (henceforth we refer to neurons exhibiting this property as beta- and theta-coherent, respectively; Figure 3). Beta-coherent neurons (n = 50; 36.8%) showed significant increases in coherence in the frequency range between 16.1 and 24.4 Hz (SFC permutation test, $p < 0.05$). Theta-coherent neurons (n = 43; 31.6%) showed cue-evoked changes in coherence between 2.9 and 9.2 Hz (SFC permutation test, $p < 0.05$). The observed SFC results were not simply driven by variations in LFP power (Supplementary Figure 3).

Moreover, we observed a prominent phase code for decision conflict in these temporally coherent neurons. We measured the mean phase at which neurons fired in relation to the population LFP for those neurons whose significance cluster overlapped with the time window used to assess firing rate selectivity. We found a clear pattern of dependence on the amount of decision conflict in both theta- and beta-coherent neurons (Figures 3c,g). Neurons generally fired before the LFP trough during high conflict trials (i.e., theta-coherent neurons fired before the theta trough and beta-coherent neurons fired before the beta trough) and after the LFP trough during low conflict trials (Figures 3d,h). The number of neurons that

Author Manuscript Author Manuscript Author Manuscript Author Manuscript

showed a phase-specific temporal code for decision conflict was larger than the number that showed a conventional rate code (McNemar's Test, $p < 10^{-3}$, $\chi^2 = 13.5$, Figure 3i). Furthermore, the phase code and rate code were largely independent from each other: rate-coding neurons seldom showed a phase code, and vice versa (correlation between firing-rate code and theta temporal code: $\rho = 0.03$; $p = 0.76$; correlation between firing-rate code and beta temporal code. $\rho = -0.02$; $p = 0.74$; Figure 3j,k). These results show robust and widespread temporal coding of decision conflict in dACC, particularly evident as a phase code, and independent of a co-existing and less prevalent rate code.

Relationship between dACC spiking activity and broader network LFP activity

We next addressed the question of how these largely distinct neuronal populations with different information-encoding strategies differentially participate in the implementation of controlled decisions. To do so, we examined their interactions with the broader network that has previously been implicated in cognitive control, which includes the dorsolateral prefrontal cortex (dlPFC). We examined the spike-triggered LFP (stLFP) of dACC neurons to determine the relationship between dACC spiking activity and local dACC LFP as well as distant dlPFC LFP (e.g. Figure 1a; recording locations for each patient are shown in Supplementary Figure 4).

The average stLFP of dACC spikes with dACC LFP ("dACC-dACC stLFP") showed a consistent deflection starting immediately after the spike and became maximally negative around 100 ms post-spike (Figure 4; all neuron categories shown in Supplementary Figure 5). The stLFP amplitude for the rate coding neurons was significantly greater than that for the beta- or theta-coherent neurons, which in turn was significantly greater than that of the non-coding neurons and null distribution (Figure 4a–c).

Spiking activity in dACC also interacted with LFP in dlPFC. SFC analysis between dACC spikes and dlPFC LFPs again revealed prominent temporal coding, with both beta- and theta-coding neuronal populations (Supplementary Figure 6). DACC spikes were also associated with significant deflections in dlPFC LFP ("dACC-dlPFC stLFP") (Figure 4d,e). These stLFP followed a similar pattern as in dACC-dACC stLFP: greatest in rate coding neurons, less but still significant in beta- and theta- phase-coding neurons, and non-significant in non-coding neurons (Figure 4f). More dACC units were coherent with dlPFC theta (49 units; 36.0%; mean significant frequency range: 2.9 – 10.2 Hz; permutation tests, $p < 0.05$), than they were with dlPFC beta (43 units; 31.6 %; mean significant frequency range for beta: 18.1 – 25.9 Hz permutation tests, $p < 0.05$). The dACC- dlPFC phase code appeared arose slightly later in beta-coherent neurons (Supplementary Figure 6a,b; significant time range: 0.8 – 2.4 s post stimulus) and slightly earlier in theta-coherent neurons (Supplementary Figure 6c,d; significant time range: 0.1 – 2.5 s post stimulus). The effect sizes for these dACC neurons that are coherent with dlPFC LFPs are shown in Supplementary Figures 6e,f. The subpopulations of dACC neurons that cohered with beta and theta-range LFPs in dlPFC were mostly distinct from those that cohered with dACC, yet their proportions did not differ significantly (Supplementary Figure 6g; McNemar's Test, $p = 0.86$, $\chi^2=0.03$). These results indicate that spiking activity in a relatively small group of

Author Manuscript Author Manuscript Author Manuscript Author Manuscript

dACC neurons (i.e. rate-coding neurons) is correlated with increased post-synaptic activity in a broader prefrontal network encompassing dACC and dlPFC.

Rate and temporal coding of task-relevant variables in dlPFC

In order to determine whether the previous findings were unique to dACC, we next tested for the presence of similar temporal coding schemes in dlPFC. We recorded single units and LFP from dlPFC in a second cohort of 9 neurosurgical subjects: 8 patients undergoing deep brain stimulation (DBS) surgery with microelectrode recordings and a subdural ECoG strip using a standard entry point over dlPFC, and one undergoing epilepsy monitoring with prefrontal subdural grid/strip electrodes and a Utah microelectrode array (UMA) in dlPFC (Figure 5a). Behavioral performance on the MSIT was similar in this cohort compared to the first (Supplementary Figure 7).

We recorded a total of 367 single units from dlPFC in these 9 subjects (Figure 5). We analyzed the same time epoch (250–750 ms after cue presentation) as we did in the dACC analysis above. Using the same sliding GLM approach to test for firing-rate selectivity, we found a small proportion of neurons encode conflict (n = 15, 4.1%). This proportion was not significantly greater than chance (exact test; $p > 0.05$) and, not surprisingly, was significantly smaller than the proportion found in dACC (χ^2 test, $\chi^2 = 8.2$, $p = 4.3*10^{-3}$). Additionally, 18 neurons were selective for response identity (4.9%; Supplementary Figure 8a) and 24 for feedback valence (6.5 %; Supplementary Figure 8b; Figure 5b).

Spike-field coherence analysis revealed prominent theta-range SFC in a large majority of recorded neurons (n = 238, 64.9%). The strength of coherence between spike timing and theta oscillations increased with higher levels of conflict (Figure 5d,e,f). This effect was prominent enough to be visible across the entire population of recorded neurons (Figure 5g) and was significant at the individual neuron level in a majority of cells (n = 191, 52.0%). Furthermore, we observed this pattern in neurons from each of the 9 subjects ($\mu \pm \sigma$ = 67.3% ± 19.9% of neurons from each subject). In contrast to its prominence in dlPFC, only a minority of dACC neurons exhibited similar conflict-modulated scaling in SFC amplitude (Fisher's exact test, $p < 10^{-5}$). On the other hand, the prominent phase-coding motif evident in dACC was not apparent in dlPFC. We find a slight precession of the SFC phase in ALL conditions, with similar error across conditions, yet no significant differences among phases for each condition. This means that the mean phase does not differ among conflict conditions, though the amplitude of SFC increases (Supplementary Figure 9c). Thus, we observed a similar general theme of uncommon rate coding but robust temporal coding in dlPFC, but the specific temporal coding schemes differed between dACC and dlPFC neurons. The overall thematic similarities demonstrate that the temporal coding archetype is not unique to dACC and suggest that temporal coding may be a conserved strategy across PFC. This finding also underscores the value of asking not only *whether* certain types of information (e.g. conflict[9]) are encoded in different PFC regions, but also *how* they are encoded.

Author Manuscript Author Manuscript Author Manuscript Author Manuscript

Trial-to-trial variation in temporal coding and its relationship to behavior

Neural information processing should be stable against noise yet flexible enough to meet unforeseen changes in cognitive demands, whether driven by external conditions or by internal fluctuations in arousal, attention, or goals[36]. Because these demands vary on a moment-to-moment basis, their trial-to-trial encoding should be detectable. We reasoned that a temporal coding scheme, distributed over a population of neurons, may be able to effectively support such an on-demand, within-trial implementation of controlled responses.

Utilizing sessions with >100 simultaneously recorded neurons, we thus considered whether a distributed population of neurons can encode a particular instance of conflict as a coherent population. We examined SFC among all simultaneously recorded dlPFC neurons during each trial and again found significant spike-theta coherence that increased in trials with higher levels of conflict (Figure 6a). Measuring SFC at the single-trial level also afforded the opportunity to examine whether trial-to-trial variation in SFC can account for trial-to-trial variation in behavior. This analysis revealed that the duration of theta coherence predicted RT on each trial (LMM, $t_{886} = 2.9$, $p = 0.002$). Furthermore, higher mean theta coherence across neurons during a given trial strongly predicted shorter RTs on that trial, even after controlling for conflict level in the current trial, in the previous trial, and their interaction (Figure 6b; theta coherence: $t_{883} = -4.22$, $p = 2*10^{-5}$). In order to control for any differences between LFP recorded from surface ECoG, and intraparenchymally recorded LFP, we examined within-trial SFC using down-sampled and filtered the LFP across the UMA between 1 and 50 Hz. Similar within-trial SFC effects were observed using intraparenchymally recorded LFP (Figure 6c; LMM, $t_{769} = -3.9$, $p = 9.5*10^{-5}$). Despite their well-established relationship to RT, all other effects in the model (current and previous trial conflict level and their interaction) were substantially weaker than the theta-coherence effect on RTs ($t_{883} \leq |1.99|$, $0.065 > p > 0.045$). Higher mean coherence was unrelated to conflict level in the previous trial ($p = 0.24$), also supporting the notion that the relationship between mean theta coherence and RTs was not driven by behavioral adaptations due to previous-trial effects[46]. These results show that a temporal code distributed across a population of dlFPC neurons closely tracks moment-to-moment fluctuations in performance, including and beyond those imposed by the task, potentially supporting a mechanism that permits flexible adjustments to cognitive demands.

Discussion

We examined responses of single neurons and LFP in two brain regions, the dACC and dlPFC, in human neurosurgical patients performing a conflict task. We found a small but significant population of neurons in dACC (but not dlPFC) whose changes in firing rate encode task conflict. While our previous report demonstrated conflict encoding at the level of a population of human dACC neurons[37], our current observation of explicit conflict encoding at the level of individual neurons has not previously been reported in humans. Our new finding is important because it is inconsistent with the idea that ostensible conflict signals in mass action measures (such as BOLD) are an epiphenomenon[13]. The firing rate encoding of conflict in these neurons was most apparent before the decision occurred, suggesting it may reflect conflict monitoring in the service of on-line control, rather

Author Manuscript Author Manuscript Author Manuscript Author Manuscript

than learning or trial-to-trial adjustment. More prominently, we found more widespread population encoding of conflict in the form of modulation of spike timing relative to ongoing LFPs. That is, a robust temporal code for decision conflict complements the more limited rate code. This temporal code appears to be independent of the spike code. Specifically, we observed this temporal code in neurons that did not exhibit a measurable firing rate code, and the magnitudes of the two codes were independent across neurons.

An emerging concept bridging these perspectives is that the relationship between neuronal spiking and ensemble oscillatory activity is a critical feature the brain uses to encode complex functional representations. Perhaps the most celebrated example of spike-oscillation synchrony is the theta phase precession observed in rat hippocampal and entorhinal "place cells"[38,39]. Similar temporal codes underlie encoding of complex visual stimuli in primary visual cortex[40], acoustic stimuli in auditory cortex[36], and coordination of gaze and reaching movements in parietal cortex[41]. It appears that there are similar neural representations of cognitive variables and spatial maps in human ACC and mesial temporal lobe[42], respectively, and that both are linked to theta rhythmicity and phase coding[43]. Recent theoretical work has proposed a dynamical control mechanism for phase coding, thus providing explanatory power and opportunities for testing specific hypotheses[44]. These factors, together with the wide-ranging interconnected nature of the medial PFC, suggest that temporal coding in the medial PFC could both be a prominent coding scheme, and support a dynamical, distributed mechanism for influencing a diverse array of brain areas[45].

Some previous work suggests that the dACC may integrate control-related variables into a general control signal and that the dlPFC may implement their effects; that is, the dACC may be, in essence, a monitor and the dlPFC may be a controller[2,46]. Our results here are broadly consistent with that proposed division of labor. First, in contrast to the dACC, we found a minimal effect of conflict on firing rate changes in dlPFC neurons, as if dlPFC does not need to signal conflict *per se*. We did find a strong oscillatory code for conflict in dlPFC, although it differed qualitatively from the one observed in dACC: it was an increase in spike-field coherence without a concurrent alignment to phase such as that observed in dACC. Oscillatory dynamic processes expand the coding space to allow optimized information formatting and consequently facilitate sparsening of downstream representations, while simultaneously conferring stability of representations in the presence of noise[36]. From this perspective, a natural interpretation is that dACC plays an upstream function, closer to the input (i.e. the source of conflict), such as a detection or signaling role. Indeed, theoretical work shows that impulses occurring at earlier phases of the cycle exert more control on the system[44]. That this phase relationship was not apparent in dlPFC is consistent with the idea that it is functionally downstream of dACC. In the same vein, theta-SFC coding in dlPFC suggests its involvement in the downstream implementation of controlled behavior, particularly given that theta coherence is strongly correlated with faster responses even after controlling for external, task-derived demands, such as amount of conflict in the current or previous trial cue. This finding accords with the idea that spike-theta coherence in dlPFC may be a "*lingua franca*" to support the implementation of controlled decision making strategies, adjusting to the presence of sources of interference regardless of whether they are external (e.g., the task or environment) or internal (e.g., spontaneous attentional fluctuations)[30,31].

Author Manuscript Author Manuscript Author Manuscript Author Manuscript

A good deal of research examining the neural bases of conflict detection and resolution has occurred in non-human animals. Classically, much of this work reported no such correlates and suggested that ostensible conflict coding may be an epiphenomenon[13,47]. In contrast, at least two recent studies suggest frank encoding of conflict may be observed in single neurons in non-human animals[48]. How can these results be reconciled? Our work suggests that two factors may be at play. First, the conflict coding observed in dACC is greatest in the temporal, phase-locked domain, and is much weaker in the rate domain, meaning that it may have been hard to detect in some studies. Indeed, the hemodynamic correlates of conflict may be more strongly linked to the oscillatory patterns we observe than to the more modest rate code. Second, the weakness of the signal in animals may be compounded by the need for over-training, which makes controlled behavior more automatized and may reduce the size of any neural signals. This effect would explain why firing rate effects appear larger in humans than in animals[37]. If so, this example illustrates one of the major benefits of human intracranial recordings: that they allow for studies of rapidly and flexibly learned behaviors[25].

Predictions from this proposed functional specialization model can be tested with future work, including simultaneous recordings of larger neuronal populations in dACC in order to measure the temporal structure of population representations, or performing closed-loop single pulse electrical stimulation at particular LFP phases in order to dynamically modulate cognitive control. Finally, this idea of functional “specialization” is specifically not meant to imply a strict functional “segregation” between dACC and dlPFC. The overall utilization of sparse rate-coding and widespread temporal-coding schemes highlights the need for an integrated understanding of the role of various neural coding strategies across prefrontal networks[45].

Conclusion: the soloists and the choir

Perhaps the most intriguing finding in our study is that the conflict rate-coding neurons, despite their low numbers, were associated with a disproportionately large relationship with LFP throughout the prefrontal network. We conjecture that this rate-coding minority may serve a specialized function of being particularly sensitive in detecting and signaling changes in conflict or, possibly, in demand for control. In other words, conflict-sensitive neurons may function as specialized “soloists” in medial PFC[49]. These soloists may serve as an early signal for the need to establish control, and then catalyze more widespread oscillatory activity throughout the network[45]. The larger population of temporal coding neurons may then act as a “choir” that stabilizes and amplifies the representation of task-relevant information. If this speculation is correct, then the soloist neurons may serve a local, intra-areal purpose, and the resulting oscillatory activity may serve to coordinate cross-regional coherent responses. This second form of responding would presumably be more robust to noise and more sensitive to regulation by top-down factors. This multi-faceted approach to representing relevant information may facilitate its efficient utilization and communication across neuronal systems.

Author Manuscript Author Manuscript Author Manuscript Author Manuscript

Materials and Methods

Subjects and ethics statement

Two cohorts of subjects participated in this research. One (Cohort 1; Methods Table 1) was a cohort of 6 patients (1 female) with medically refractory epilepsy who were undergoing intracranial monitoring to identify seizure onset regions. These subjects had been implanted with stereo-encephalography (sEEG) depth electrodes using standard stereotactic techniques. One or more of the sEEG electrodes in this cohort spanned dorsolateral prefrontal cortex (dlPFC) to dorsal anterior cingulate cortex (dACC; Brodmann's areas 24a/b/c and 32), providing LFP recordings from both regions, as well as single unit recordings in dACC (see below; Data Acquisition).

The other (Cohort 2; Methods Table 2) was a cohort of 9 patients: 8 (2 female) with movement disorders (Parkinson's disease or essential tremor) who were undergoing deep brain stimulation (DBS) surgery, and one male patient with epilepsy undergoing intracranial seizure monitoring. The entry point for the trajectory of the DBS electrode is typically in the inferior portion of the superior frontal gyrus or superior portion of the middle frontal gyrus, within 2 cm of the coronal suture. This area corresponds to dlPFC (Brodmann's areas 9 and 46). The single epilepsy patient in this cohort underwent a craniotomy for placement of subdural grid/strip electrodes in a prefrontal area including dlPFC. Thus this cohort provided single-unit and LFP recordings from dlPFC (see below; Data Acquisition).

All decisions regarding sEEG and DBS trajectories and craniotomy location were made solely based on clinical criteria. The Columbia University Medical Center Institutional Review Board approved these experiments, and all subjects provided informed consent prior to participating in the study.

Behavioral Task

All subjects performed the multi-source interference task (MSIT; Figure 1b)[50], in which each trial consisted of a 500-millisecond fixation period, followed by a cue consisting of three integers ranging from 0 to 3. One of these three numbers (the "target") was different from the other two numbers (the "distractors"). Subjects were instructed to indicate the identity of the target number on a 3-button pad, upon which each button represented the integers 1 (left button), 2 (middle) and 3 (right), respectively. This task therefore presented two types of conflict: spatial conflict if the target was in a different position in the cue than on the 3-button pad (i.e. '0 0 1'; target in right position, but left button is correct choice), and distractor conflict if the distractor numbers were possible button choices (e.g. '3 2 3', in which "3" corresponds to a possible button choice; vs. '0 2 0', in which "0" does not correspond to a possible button choice). After each subject registered his or her response, the cue disappeared and feedback appeared, consisting of the target number in a different color, with a variable delay of 300 to 800 milliseconds. Valenced feedback (green/red for correct/incorrect, respectively) alternated with neutral feedback (blue regardless of correctness) in blocks of 10 trials. The intertrial interval varied uniformly randomly between 1 and 1.5 seconds.

Author Manuscript Author Manuscript Author Manuscript Author Manuscript

The task was presented on a computer monitor controlled by the Psychophysics Matlab Toolbox (www.psychtoolbox.org; The MathWorks, Inc). This software interfaced with data acquisition cards (National Instruments,) that allowed for synchronization of behavioral events and neural data with sub-millisecond precision. Differences in log RTs over conflict conditions were tested using mixed effects models (LMM)

$$\boldsymbol{y} = \boldsymbol{X}\beta + \boldsymbol{Z}\boldsymbol{u} + \epsilon$$

where $\boldsymbol{y}$ represents RTs, $\boldsymbol{X}$ represents a design matrix of conflict condition factors, β represents the fixed effects regression coefficients, $\boldsymbol{Z}$ represents the random effects design matrix accounting for random variance in subject-session RTs, $\boldsymbol{u}$ represents the random component of the fixed effects in β, and ϵ represents the model residuals, or in Wilkinson notation, RT ~ 1+ conflict condition*session + (1 + conflict condition*session | subject). RTs were lognormally distributed, so we modeled the log of RT in order to meet assumptions of normality. These models were fit using maximum likelihood methods using the Matlab function fitglme. Subsequent linear models are specified using Wilkinson notation.

Statistics

As described in the previous section, many of the hypotheses were tested with LMMs whose main effects were evaluated with two-sided t-tests. All statistical tests performed are listed in Supplementary Table 4. For tests that assumed normality, a priori Lilliefors tests were performed in order to confirm that data were normally distributed. Sample sizes were based on numbers of trials and neurons, both of which were randomized. The number of trials was determined by the patients' willingness and motivation to perform the task. The conflict type for each trial was randomly assigned from a uniform distribution. The number of neurons was based on where microelectrodes ended up recording, approximately 4 mm away from the nearest macroelectrode, which was placed based on clinical parameters. Experimenters were neither able to control the number of trials a patient performed, nor the precise location of microelectrodes, nevertheless we report similar numbers to previous studies[37,51–53]. Data collection and analysis were not performed blind to the conditions of the experiments. Additional Information may be found in the Life Sciences Reporting Summary.

Data Acquisition and preprocessing

Data were acquired at two electrophysiological scales from each subject: single unit activity (SUA), and local field potentials (LFP). SUA was recorded from microelectrodes using 3 different techniques. In Cohort 1, the dlPFC-dACC sEEG electrodes were "Behnke-Fried" macro-micro electrodes (AdTech Medical), which consist of a standard clinical depth macroelectrode shaft with a bundle of eight shielded microwires that protrude ~4 mm from the tip (IRB-AAAB6324). These 8 microwires are referenced to a ninth unshielded microwire. dACC SUA was acquired with this technique (Figure 1b, 2a). Cohort 2 provided dlPFC SUA using 2 techniques (Figure 5a). The DBS surgeries were performed according to standard clinical procedure, using clinical microelectrode recording (FHC). Prior to inserting the guide tubes for the clinical recordings, we placed the microelectrodes in the cortex under direct vision to record from dlPFC, as we have previously described (IRB-AAAK2104)[52].

Author Manuscript Author Manuscript Author Manuscript Author Manuscript

The epilepsy implant in Cohort 2 included a Utah-style microelectrode array (UMA) implanted in dlPFC (IRB-AAAB6324), as we have previously described[54–56]. Data were amplified, high-pass filtered, and digitized at 30 kilosamples per second on a neural signal processor (Blackrock Microsystems, LLC) simultaneously with the ECoG data.

LFP were recorded from subdural electrocorticography (ECoG) electrodes or standard clinical sEEG macroelectrodes. In Cohort 1, LFP data were recorded from the eight contacts along the clinical ECoG electrode and referenced to either a scalp electrode or a quiescent sEEG contact in the cerebral white matter, depending on the clinical recording configuration. The medial contacts were within dACC, and lateral contacts within dlPFC (Figure 1a). In the DBS patients in Cohort 2, LFP data were recorded from 8-contact (3 mm electrode diameter, 5 mm inter-contact spacing) ECoG strips (PMT Corporation). These ECoG strips were slid over the cortical surface through the burr hole adjacent to the microelectrodes and were referenced to scalp needle electrodes adjacent to the mastoid bone. For the epilepsy patient in Cohort 2, LFP data were recorded from the nearest ECoG electrode on the grid overlying the UMA and referenced to an epidural ECoG strip. In all cases, signals from ECoG contacts were pseudodifferentially amplified by ten and digitized at two kHz on the same recording system, and therefore same time base, as the SUA and task event data.

LFP data were preprocessed by first removing clearly broken ECoG or sEEG electrodes and then removing the common mode across channels by reconstructing the data without its first principal component. The resultant time series were then epoched from two seconds before until three seconds after the time of stimulus onset. Trials containing epileptiform discharges were removed based on the range of the LFP voltage across all trials. Those trials in which the range of the signal was greater than 1.5 times the interquartile range of the distribution of voltage ranges across all trials were manually reviewed and excluded. LFP spectra between 0 and 150 Hz were calculated using multitaper methods using the Chronux toolbox for Matlab with 5 leading tapers and a time-bandwidth product of 3.

Action potential sorting

SUA data were re-thresholded offline at negative four times the root mean square of the 250 Hz high-pass filtered signal. Well-isolated action potential waveforms were then segregated in a semi-supervised manner using the T-distribution expectation-maximization method on a feature space comprised of the first three principal components using Offline Sorter software (Plexon Inc, Dallas, TX; USA)[57]. The times of threshold crossing for identified single units were retained for further analysis.

Classification of single unit selectivity

In order to estimate neuronal selectivity, we fit a sliding GLM (using similar methods to[10]) to the normalized firing rate of each neuron averaged over a time window of 250 ms each, and repeated this process iteratively, shifting in steps of 20 ms for the duration of the whole trial. This GLM, implemented with custom scripts in Matlab (MathWorks, Inc), consisted of a 3-way ANOVA with factors: decision conflict (4 levels: neither conflict, spatial conflict, flanker conflict, and both), response identity (3 levels: button 1, 2, or 3), and feedback

Author Manuscript Author Manuscript Author Manuscript Author Manuscript

valence (2 levels: neutral vs. valenced feedback). This ANOVA model also accounted for reaction time as a nuisance variable and included interaction terms for all 4 factors. Using this sliding GLM, we classified individual neurons based on their firing rate selectivity for these task-relevant features.

We focused our analyses on target windows of 500 ms during a post-cue period centered 500 ms after the cue onset rather than on longer time windows so as to limit the number of statistical tests. To establish statistical significance while controlling for multiple tests within each target window (i.e., one test for each of 25 20-ms steps), we performed a permutation test in which trains of neuronal spike data corresponding to a trial were randomly reshuffled across trials, for each of the neurons separately, for a total of 10,000 iterations. Using the main 3-way ANOVA model with test windows of 250 ms and steps of 20 ms, a combined threshold of $p \leq 0.03$ for at least 4 consecutive steps yielded significant effects for the first factor (in a 500-ms target window) in less than 5% of the surrogate neurons. The alpha value of 0.03 was chosen in order to correct for the number of consecutive bins required to reach significance and corresponds to a corrected alpha value of 0.05. This combined significance threshold, which had the higher yet significant p-value combined with longer duration, was chosen over a combined threshold of lower p-value with shorter duration because meaningful electrophysiological effects (true positives) tend to last for several consecutive time-points in contrast with noisy effects (false positives). We thus adopted this combined height-duration threshold in all our analyses of individual neurons to control for multiple comparisons. McNemar's test with a Yates' corrected χ^2 were used to test for differences in proportions of neurons. All tests were two-sided.

Spike-Field Coherence

Spike-field coherence (SFC) was calculated using multi-taper methods using the Chronux toolbox for matlab[58]. SFC coherograms were generated using a one-second window size, a 10 millisecond step size, a time-bandwidth product of five, and nine leading tapers. Significant changes in coherence were determined with permutation tests, where random trials of SUA and LFP data were paired. Such a randomized trial pairing was performed 10,000 times, and SFC was recalculated between random pairs of SUA and LFP data in order to generate SFC null distributions. Coherograms for each neuron and condition (randomly subsampling numbers of trials such that they were balanced across conditions) were then tested against these null distributions in order to determine statistically significant frequency bands and time ranges using cluster corrected permutation tests with significance levels of 0.05[59]. Only significant clusters following the onset of the stimulus and before the maximum RT were considered. We refer to this procedure as the SFC permutation test in the main text. The phase and amplitude of coherence among conditions were then examined for neurons exhibiting significant SFC clusters. In order to enable comparison with the firing rate models, these phase or reliability coding effects were assessed using a sliding ANOVA over the same time epoch as that for which firing rate effects were assessed, specifically 250–750 ms following stimulus onset[59].

Single-trial coherence for the UMA data was calculated as described above, except that coherence was calculated across simultaneously-recorded neurons for each trial. Ordinary

Author Manuscript Author Manuscript Author Manuscript Author Manuscript

least squares linear regression was used to predict RTs in each condition from single-trial theta coherence calculated amongst simultaneously-recorded dlPFC neurons. In order to confirm that the amount of decision conflict on previous trials did not affect our ability to predict RT from single trial coherence across a population of dlPFC neurons, we implemented a multiple regression model of RT using theta coherence, current trial conflict level, previous trial conflict level, and the interaction between current and previous trial conflict levels as predictors (RT ~ 1 + theta coherence + current trial conflict level * previous trial conflict level).

Discriminability

In order to roughly compare the time courses of conflict effects across coding schemes, we fit a linear discriminant model to each time point of the firing rate or coherence phase data across populations of each category of neuron[60]. This model was evaluated with four-fold cross-validation and a permutation threshold based on reshuffling conflict labels among trial data was used to determine significance (values greater than 95% of the area under the permutation distribution).

Spike-Triggered Local Field Potentials

In order to understand the average influence of a dACC neuron's action potential on population synaptic dynamics in dACC and dlPFC, we aligned three seconds of LFP recorded in dACC and dlPFC before and after the time of each dACC spike occurring between 250 ms and 750 ms following the cue. These LFPs were decorrelated by their covariance matrix and then z-scored. Averaging these LFPs generated a spike-triggered local field potential (stLFP). stLFPs have been shown to be closely related to the cross correlation of the intracellularly recorded membrane potential and the surrounding LFP[61]. To generate null distributions to test for any stLFP effect, while maintaining both the temporal structure in the population firing rate and each neuron's contribution to the mean population firing rate overall, spikes were also randomly shifted among adjacent 1 ms time bins and across adjacent trials using the raster margins model[62]. Null distributions for stLFP were generated by calculating stLFPs from these shifted spike times and the original LFP as described in the raster margins model. stLFP amplitude was operationally defined as the minimum stLFP during the 200 ms following the mean dACC spike time. Again a LMM was utilized to assess significance among stLFPs that were associated with particular classes of neurons. The model specification in this case was: stLFP ~ 1 + conflict-selective neurons*session + theta-coherent neurons*session + beta coherent neurons*session + non-coding neurons*session + (1 + conflict-selective neurons*session + theta-coherent neurons*session + beta coherent neurons*session + non-coding neurons*session | subject).

Code availability

All analysis code is available online at http://www.github.com/elliothsmith/MSIT-analysis

Supplementary Material

Refer to Web version on PubMed Central for supplementary material.

Author Manuscript Author Manuscript Author Manuscript Author Manuscript

Acknowledgements

This work was supported by NIH R01 MH106700 (S.A.S.), NIH K12 NS080223 (S.A.S.), NIH S10 OD018211 (C.A.S.), NIH R01 NS084142 (C.A.S.), NIH R01 DA038615 (B.Y.H.), the Dana Foundation (S.A.S.), the McNair Foundation (S.A.S.), and a Young Investigator grant from the Brain & Behavior Research Foundation (E.H.S). Special thanks to C. Casadei, D. K. Peprah, and T. G. Dyster for coordination and data collection efforts.

References

1. Botvinick M & Braver T Motivation and Cognitive Control: From Behavior to Neural Mechanism. Annu. Rev. Psychol 66, 83–113 (2015). [PubMed: 25251491]
2. Shenhav A et al. Toward a Rational and Mechanistic Account of Mental Effort. Annu. Rev. Neurosci 40, 99–124 (2017). [PubMed: 28375769]
3. Miller EK & Cohen JD An Integrative Theory of Prefrontal Cortex Function. Annu. Rev. Neurosci 24, 167–202 (2001). [PubMed: 11283309]
4. Abi-Dargham A & Horga G The search for imaging biomarkers in psychiatric disorders. Nat. Med 22, 1248–1255 (2016). [PubMed: 27783066]
5. Cole MW, Repovš G & Anticevic A The frontoparietal control system: a central role in mental health. The Neuroscientist 20, 652–664 (2014). [PubMed: 24622818]
6. Horga G et al. Adaptation to Conflict via Context-Driven Anticipatory Signals in the Dorsomedial Prefrontal Cortex. J. Neurosci 31, 16208–16216 (2011). [PubMed: 22072672]
7. Blanchard TC, Strait CE & Hayden BY Ramping ensemble activity in dorsal anterior cingulate neurons during persistent commitment to a decision. J. Neurophysiol 114, 2439–2449 (2015). [PubMed: 26334016]
8. Botvinick M, Nystrom LE, Fissell K, Carter CS & Cohen JD Conflict monitoring versus selection-for-action in anterior cingulate cortex. Nature 402, 179–181 (1999). [PubMed: 10647008]
9. Carter CS et al. Anterior Cingulate Cortex, Error Detection, and the Online Monitoring of Performance. Science 280, 747 (1998). [PubMed: 9563953]
10. Kennerley SW, Behrens TEJ & Wallis JD Double dissociation of value computations in orbitofrontal and anterior cingulate neurons. Nat. Neurosci 14, 1581 (2011). [PubMed: 22037498]
11. Hayden BY, Heilbronner SR, Pearson JM & Platt ML Surprise Signals in Anterior Cingulate Cortex: Neuronal Encoding of Unsigned Reward Prediction Errors Driving Adjustment in Behavior. J. Neurosci 31, 4178–4187 (2011). [PubMed: 21411658]
12. Amemori K & Graybiel AM Localized microstimulation of primate pregenual cingulate cortex induces negative decision-making. Nat. Neurosci 15, 776 (2012). [PubMed: 22484571]
13. Nakamura K, Roesch MR & Olson CR Neuronal Activity in Macaque SEF and ACC During Performance of Tasks Involving Conflict. J. Neurophysiol 93, 884 (2005). [PubMed: 15295008]
14. Glascher J et al. Lesion mapping of cognitive control and value-based decision making in the prefrontal cortex. Proc. Natl. Acad. Sci 109, 14681–14686 (2012). [PubMed: 22908286]
15. Alexander WH & Brown JW Medial prefrontal cortex as an action-outcome predictor. Nat. Neurosci 14, 1338 (2011). [PubMed: 21926982]
16. Shenhav A, Straccia MA, Cohen JD & Botvinick MM Anterior cingulate engagement in a foraging context reflects choice difficulty, not foraging value. Nat. Neurosci 17, 1249 (2014). [PubMed: 25064851]
17. Kolling N et al. Value, search, persistence and model updating in anterior cingulate cortex. Nat. Neurosci 19, 1280 (2016). [PubMed: 27669988]
18. Collins AGE & Frank MJ Cognitive control over learning: Creating, clustering, and generalizing task-set structure. Psychol. Rev 120, 190–229 (2013). [PubMed: 23356780]
19. Gratton G, Coles MG & Donchin E Optimizing the use of information: strategic control of activation of responses. J. Exp. Psychol. Gen 121, 480 (1992). [PubMed: 1431740]
20. MacDonald AW Dissociating the Role of the Dorsolateral Prefrontal and Anterior Cingulate Cortex in Cognitive Control. Science 288, 1835–1838 (2000). [PubMed: 10846167]
21. Ebitz RB & Hayden BY Dorsal anterior cingulate: a Rorschach test for cognitive neuroscience. Nat. Neurosci 19, 1278 (2016). [PubMed: 27669987]

Author Manuscript Author Manuscript Author Manuscript Author Manuscript

22. Blanchard TC & Hayden BY Neurons in Dorsal Anterior Cingulate Cortex Signal Postdecisional Variables in a Foraging Task. J. Neurosci 34, 646–655 (2014). [PubMed: 24403162]
23. Wise SP Forward frontal fields: phylogeny and fundamental function. Trends Neurosci. 31, 599–608 (2008). [PubMed: 18835649]
24. Heilbronner SR, Rodriguez-Romaguera J, Quirk GJ, Groenewegen HJ & Haber SN Circuit-Based Corticostriatal Homologies Between Rat and Primate. Biol. Psychiatry 80, 509–521 (2016). [PubMed: 27450032]
25. Cole MW, Yeung N, Freiwald WA & Botvinick M Cingulate cortex: Diverging data from humans and monkeys. Trends Neurosci. 32, 566–574 (2009). [PubMed: 19781794]
26. Cole MW, Yeung N, Freiwald WA & Botvinick M Conflict over Cingulate Cortex: Between-Species Differences in Cingulate May Support Enhanced Cognitive Flexibility in Humans. Brain. Behav. Evol 75, 239–240 (2010). [PubMed: 20693782]
27. Womelsdorf T et al. Modulation of Neuronal Interactions Through Neuronal Synchronization. Science 316, 1609–1612 (2007). [PubMed: 17569862]
28. Logothetis NK, Pauls J, Augath M, Trinath T & Oeltermann A Neurophysiological investigation of the basis of the fMRI signal. Nature 412, 150–157 (2001). [PubMed: 11449264]
29. Logothetis NK & Wandell BA Interpreting the BOLD Signal. Annu. Rev. Physiol 66, 735–769 (2004). [PubMed: 14977420]
30. Cavanagh JF & Frank MJ Frontal theta as a mechanism for cognitive control. Trends Cogn. Sci 18, 414–421 (2014). [PubMed: 24835663]
31. Cavanagh JF, Zambrano-Vazquez L & Allen JJB Theta lingua franca: A common mid-frontal substrate for action monitoring processes. Psychophysiology 49, 220–238 (2012). [PubMed: 22091878]
32. Oehrn CR et al. Neural Communication Patterns Underlying Conflict Detection, Resolution, and Adaptation. J. Neurosci 34, 10438 (2014). [PubMed: 25080602]
33. Tang H et al. Cascade of neural processing orchestrates cognitive control in human frontal cortex. Elife 5, e12352 (2016). [PubMed: 26888070]
34. Helfrich RF & Knight RT Oscillatory Dynamics of Prefrontal Cognitive Control. Trends Cogn. Sci 20, 916–930 (2016). [PubMed: 27743685]
35. Pesaran B et al. Investigating large-scale brain dynamics using field potential recordings: analysis and interpretation. Nat. Neurosci 21, 903–919 (2018). [PubMed: 29942039]
36. Kayser C, Montemurro MA, Logothetis NK & Panzeri S Spike-Phase Coding Boosts and Stabilizes Information Carried by Spatial and Temporal Spike Patterns. Neuron 61, 597–608 (2009). [PubMed: 19249279]
37. Sheth SA et al. Human dorsal anterior cingulate cortex neurons mediate ongoing behavioural adaptation. Nature 488, 218 (2012). [PubMed: 22722841]
38. Jensen O & Lisman JE Position Reconstruction From an Ensemble of Hippocampal Place Cells: Contribution of Theta Phase Coding. J. Neurophysiol 83, 2602–2609 (2000). [PubMed: 10805660]
39. O'Keefe J & Burgess N Dual phase and rate coding in hippocampal place cells: theoretical significance and relationship to entorhinal grid cells. Hippocampus 15, 853–866 (2005). [PubMed: 16145693]
40. Montemurro MA, Rasch MJ, Murayama Y, Logothetis NK & Panzeri S Phase-of-Firing Coding of Natural Visual Stimuli in Primary Visual Cortex. Curr. Biol 18, 375–380 (2008). [PubMed: 18328702]
41. Hawellek DJ, Wong YT & Pesaran B Temporal coding of reward-guided choice in the posterior parietal cortex. Proc. Natl. Acad. Sci 113, 13492–13497 (2016). [PubMed: 27821752]
42. Constantinescu AO, O'Reilly JX & Behrens TEJ Organizing Conceptual Knowledge in Humans with a Grid-like Code. Science 352, 1464–1468 (2016). [PubMed: 27313047]
43. O'Keefe J & Recce ML Phase relationship between hippocampal place units and the EEG theta rhythm. Hippocampus 3, 317–330 (1993). [PubMed: 8353611]
44. Neurosystems: brain rhythms and cognitive processing - Cannon - 2014 - European Journal of Neuroscience - Wiley Online Library. Available at: https://onlinelibrary.wiley.com/doi/epdf/10.1111/ejn.12453. (Accessed: 19th February 2019)

Author Manuscript Author Manuscript Author Manuscript Author Manuscript

45. Eisenreich BR, Akaishi R & Hayden BY Control without Controllers: Toward a Distributed Neuroscience of Executive Control. J. Cogn. Neurosci 29, 1684–1698 (2017). [PubMed: 28430042]
46. Shenhav A, Botvinick MM & Cohen JD The Expected Value of Control: An Integrative Theory of Anterior Cingulate Cortex Function. Neuron 79, 217–240 (2013). [PubMed: 23889930]
47. Ito T, Tiede M & Ostry DJ Somatosensory function in speech perception. Proc. Natl. Acad. Sci 106, 1245–1248 (2009). [PubMed: 19164569]
48. Ebitz RB & Platt ML Neuronal Activity in Primate Dorsal Anterior Cingulate Cortex Signals Task Conflict and Predicts Adjustments in Pupil-Linked Arousal. Neuron 85, 628–640 (2015). [PubMed: 25654259]
49. 23 Problems in Systems Neuroscience. (Oxford University Press, 2006). doi:10.1093/acprof:oso/9780195148220.001.0001
50. Bush G & Shin LM The Multi-Source Interference Task: an fMRI task that reliably activates the cingulo-frontal-parietal cognitive/attention network. Nat. Protoc 1, 308–313 (2006). [PubMed: 17406250]
51. Fu Z et al. Single-Neuron Correlates of Error Monitoring and Post-Error Adjustments in Human Medial Frontal Cortex. Neuron 101, 165–177.e5 (2019). [PubMed: 30528064]
52. Mian MK et al. Encoding of Rules by Neurons in the Human Dorsolateral Prefrontal Cortex. Cereb. Cortex 24, 807–816 (2014). [PubMed: 23172774]
53. Jacobs J et al. Direct recordings of grid-like neuronal activity in human spatial navigation. Nat. Neurosci 16, 1188–1190 (2013). [PubMed: 23912946]
54. Schevon CA et al. Evidence of an inhibitory restraint of seizure activity in humans. Nat. Commun 3, 1060 (2012). [PubMed: 22968706]
55. Smith EH et al. The ictal wavefront is the spatiotemporal source of discharges during spontaneous human seizures. Nat. Commun 7, 11098 (2016). [PubMed: 27020798]
56. House PA, MacDonald JD, Tresco PA & Normann RA Acute microelectrode array implantation into human neocortex: preliminary technique and histological considerations. Neurosurg. Focus 20, 1–4 (2006).
57. Shoham S, Fellows MR & Normann RA Robust, automatic spike sorting using mixtures of multivariate t-distributions. J. Neurosci. Methods 127, 111–122 (2003). [PubMed: 12906941]
58. Mitra PP & Pesaran B Analysis of dynamic brain imaging data. Biophys. J 76, 691–708 (1999). [PubMed: 9929474]
59. Maris E & Oostenveld R Nonparametric statistical testing of EEG- and MEG-data. J. Neurosci. Methods 164, 177–190 (2007). [PubMed: 17517438]
60. Izenman AJ Linear Discriminant Analysis. in Modern Multivariate Statistical Techniques: Regression, Classification, and Manifold Learning (ed. Izenman AJ) 237–280 (Springer New York, 2008). doi:10.1007/978-0-387-78189-1_8
61. Okun M, Naim A & Lampl I The Subthreshold Relation between Cortical Local Field Potential and Neuronal Firing Unveiled by Intracellular Recordings in Awake Rats. J. Neurosci 30, 4440–4448 (2010). [PubMed: 20335480]
62. Okun M et al. Diverse coupling of neurons to populations in sensory cortex. Nature 521, 511 (2015). [PubMed: 25849776]

Author Manuscript Author Manuscript Author Manuscript Author Manuscript

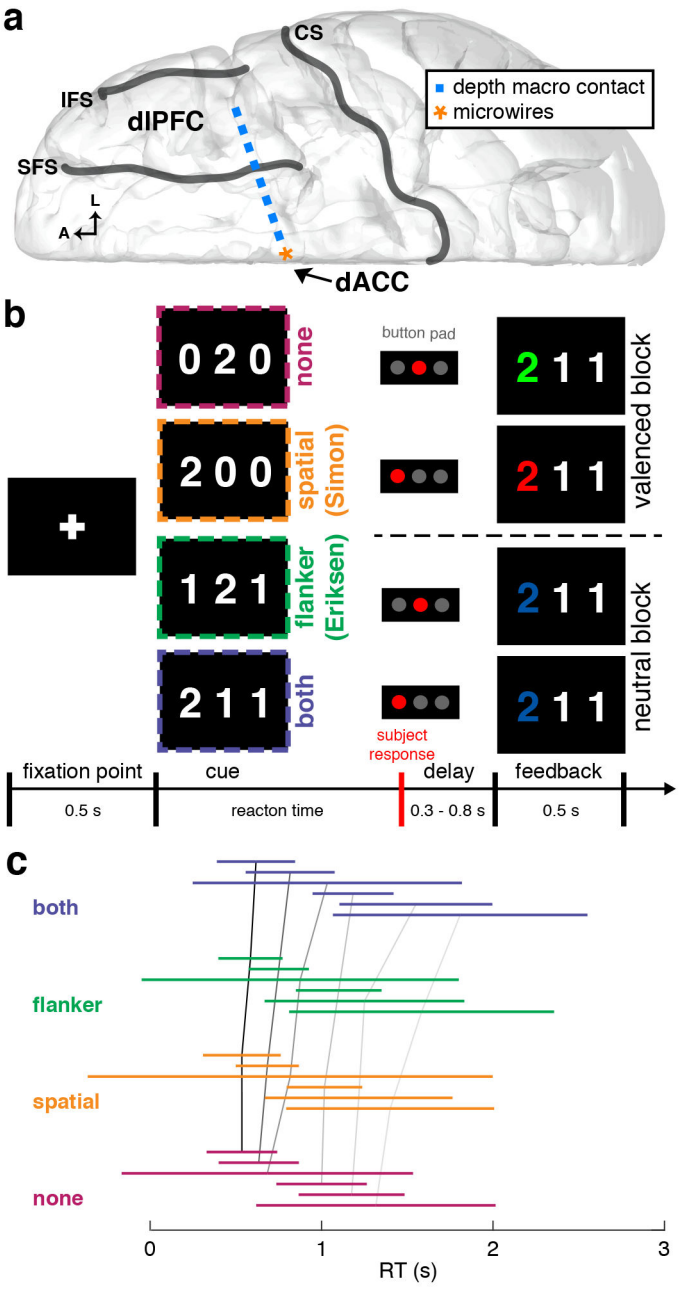

Figure 1. Recording configuration, task description, and behavioral performance |

a, Diagram of the intracranial implant including a stereotactically placed intra-cerebral depth electrode with macroelectrodes (blue squares) along the shaft from dlPFC to dACC and microwire electrodes (orange star) in dACC. A, anterior; L, lateral; CS, central sulcus; SFS, superior frontal sulcus; IFS, inferior frontal sulcus. **b,** Multi-source interference task (MSIT). The subject sees a cue consisting of 3 numbers and has to identify the unique number (“target”) and respond with a button push: left button if the target is “1”, middle if “2”, right if “3”. Incongruence between the location of the target number in the 3-digit sequence and location of the correct button in the 3-button pad produces spatial (Simon) conflict (orange). The distracting presence of numbers that are valid button choices (“1”,

Author Manuscript Author Manuscript Author Manuscript Author Manuscript

"2", "3", vs. "0", which is not a valid choice) produces flanker (Eriksen) conflict (green). Trials can also have neither type of conflict (magenta) or both types (violet). In all 4 example trials shown, "2" is the target; thus the middle button is the correct response. Following the response, valenced (green/red for correct/incorrect; 2 example trials shown above dashed line) or unvalenced (blue regardless of correctness; 2 example trials below dashed line) feedback is provided in alternating blocks of 10 trials. **c,** Line plots of RT distributions across all patient. Each colored line represents two standard deviations of RTs centered on the mean RT and color-coded each conflict condition. Black and gray lines connect the means across conflict conditions within each patient. There was a statistically significant difference among conflict conditions (generalized linear mixed effects model, $t_{3881} = 2.36$, $p = 0.01$). RT distributions for each subject and session are shown in Supplementary Figure 7.

Author Manuscript Author Manuscript Author Manuscript Author Manuscript

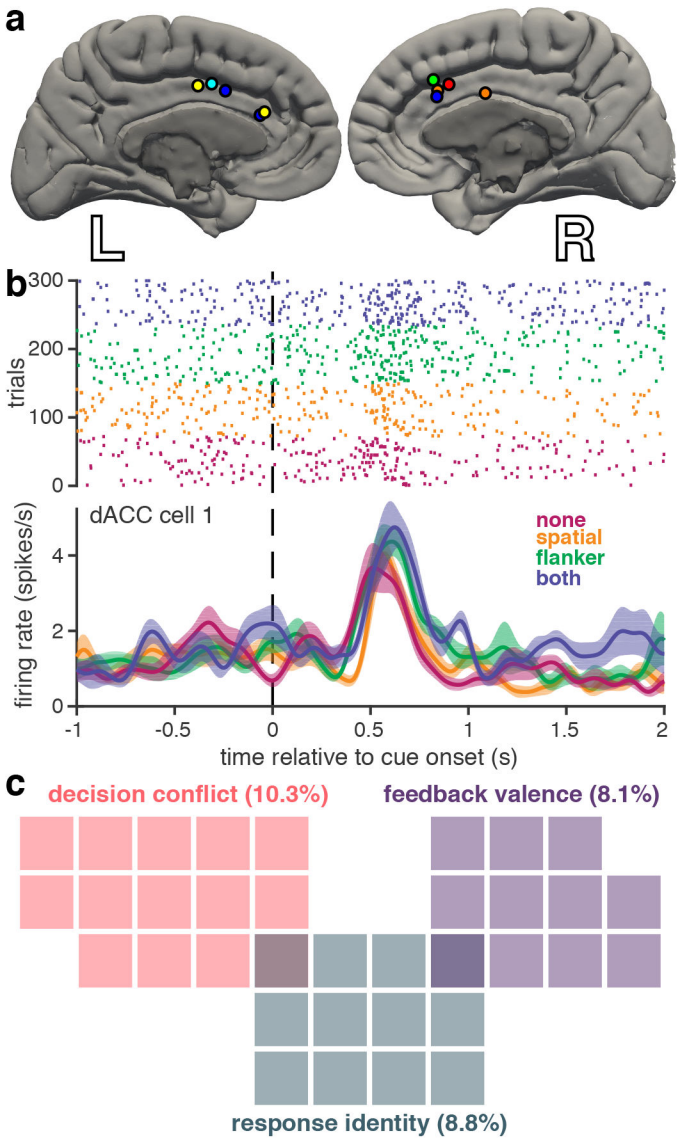

Figure 2. Rate coding of task-relevant variables in human dACC neurons |

a, Microwire recording locations, with different colors per subject. **b,** Example dACC raster plot and firing rate over conflict conditions for a representative neuron that shows rate coding for decision conflict. Conflict conditions are color-coded as in Figure 1. Shaded regions represent standard error (n = 72, 77, 85, and 66 trials for none, spatial, flanker, and both conditions, respectively). **c,** Venn diagram showing only those dACC neurons that were selective for specific task features, as determined by the sliding GLM. Each colored square represents one neuron; percentage of total n = 136 neurons indicated in parentheses.

Author Manuscript Author Manuscript Author Manuscript Author Manuscript

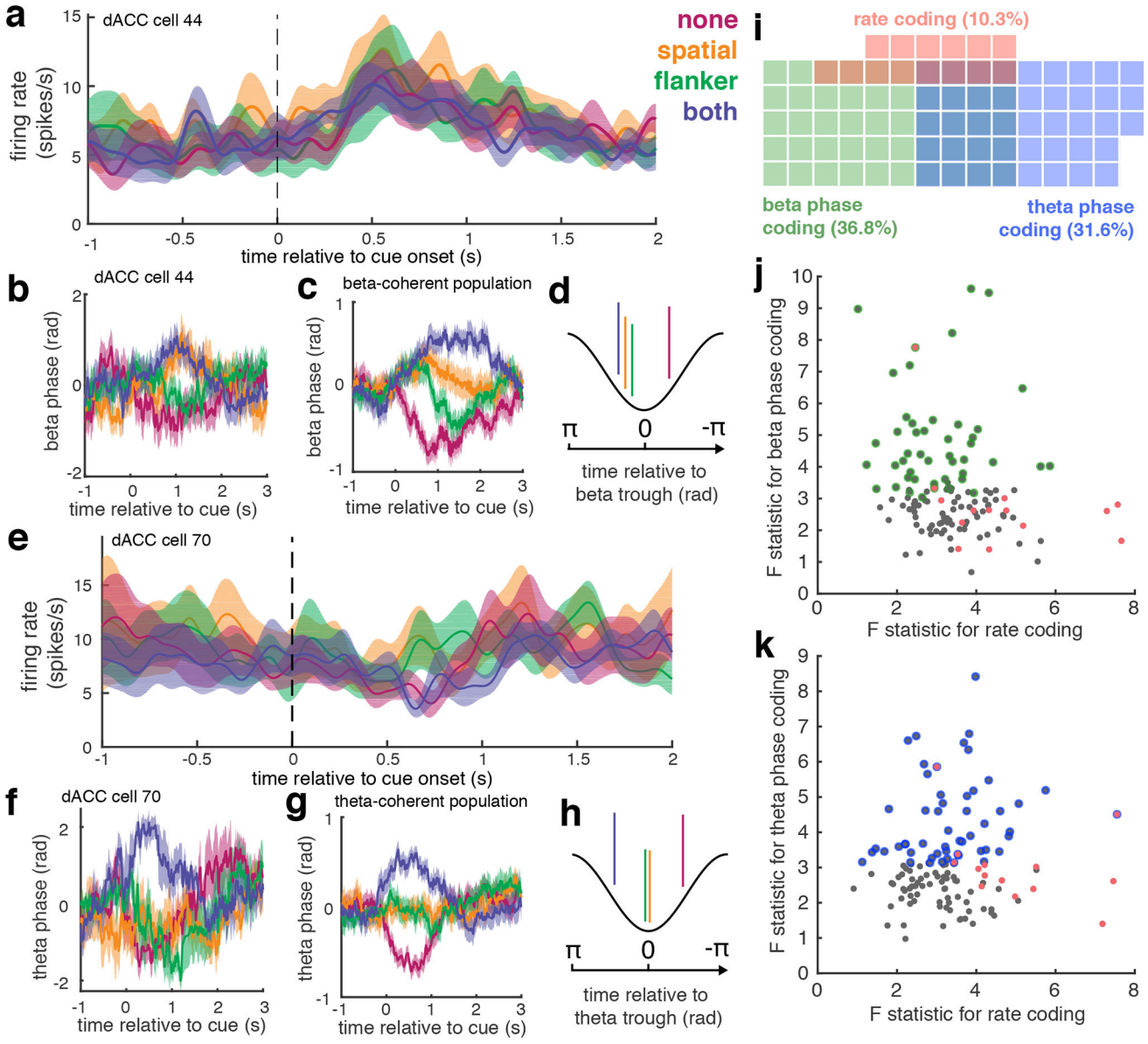

Figure 3. Robust phase coding in dACC neurons |

a, Example dACC neuron whose firing rate does not vary by conflict level (no firing rate code). **b**, Mean phase of SFC for a single beta-coherent neuron for each conflict condition. Shaded regions in **a**, and **b** represent standard error (n = 72, 77, 85, and 66 trials for none, spatial, flanker, and both conditions, respectively). **c,** Mean phase of SFC across all beta-coherent neurons color coded by conflict condition (LMM t-test, $t_{510} = 3.6$, $p = 4*10^{-4}$). Shading represents standard error across 50 beta coherent neurons. **d,** Schematic showing mean spike phase for each conflict condition in beta-coherent neurons. **e,f,** Same as **a,b** for a different dACC neuron that again shows no firing rate code, but shows increased theta coherence (N = 69 trials for each conflict condition). **g,h,** Same as **c,d**, for theta-coherent neurons (LMM t-test, $t_{510} = 3.1$, $p = 2*10^{-3}$). Shading represents standard error across 43 theta coherent neurons. **i,** Venn diagram showing only the proportions of neurons that were

Author Manuscript Author Manuscript Author Manuscript Author Manuscript

either beta phase coding (green), theta phase coding (blue), or rate coding (pink) neurons for decision conflict. The proportion of beta- or theta-phase coding neurons was significantly greater than that of rate coding neurons (73 vs 14 neurons; McNemar's Test, $\chi^2 = 13.5$, $p < 10^{-3}$). **j,k**, For each neuron, the maximum F statistic from the beta (**j**) or theta (**k**) phase code F-statistics plotted against the maximum F statistic from the firing rate GLM (Spearman's rho for theta: $\rho = 0.03$; p = 0.76; for beta: $\rho = -0.08$; p = 0.32; two-sided t-tests). Scatter plots show statistics for all 136 neurons. Significant rate coding cells are shown in pink, and significant phase coding cells are indicated with colored circles for each frequency range, as in **i**.

Author Manuscript Author Manuscript Author Manuscript Author Manuscript

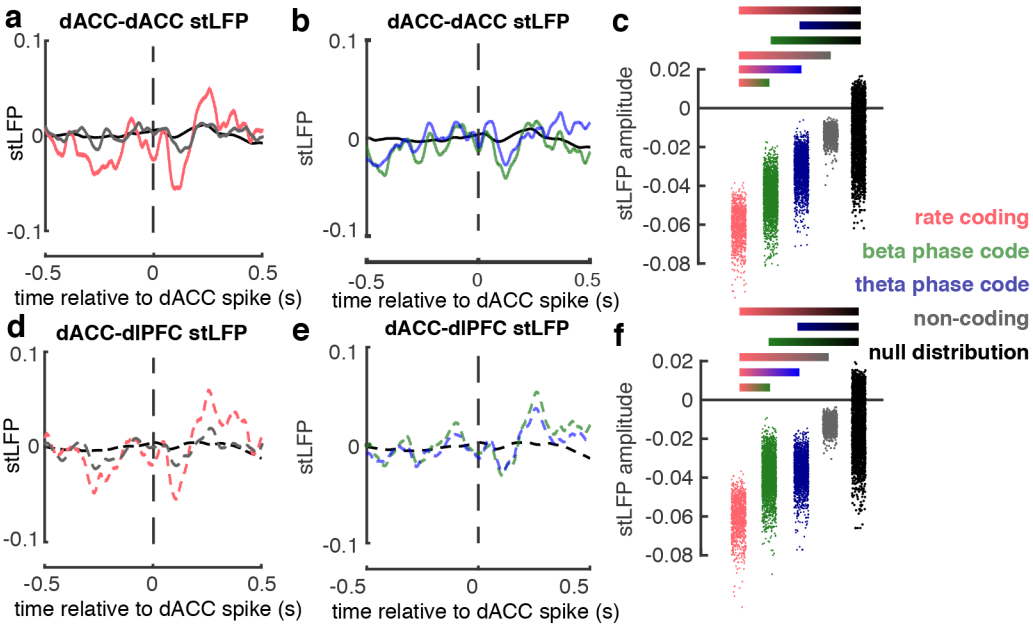

Figure 4. dACC neuronal interactions within a broader control network |

a, Spike-triggered LFP (stLFP) waveforms evoked by dACC neurons on dACC LFP ("dACC-dACC") for conflict selective rate coding neurons (red, n = 2,370 spikes), non-coding neurons (gray, n = 10,292 spikes), and null distribution (black). **b,** dACC-dACC stLFP waveforms for temporal coding neurons: beta-coherent (green, n = 8,398 spikes), theta-coherent (blue, n = 7,581 spikes), and null distribution (black). **c,** Distributions of dACC-dACC stLFP amplitudes for each neuron group in **a**,**b**. stLFP amplitudes were decorrelated by their covariance matrices and Z-scored. **d-f**, same spikes and details as in **a-c**, but for stLFP evoked by dACC neurons on dlPFC LFP ("dACC-dlPFC"). Gradient bars in **c**,**f** show significant pairwise post hoc comparisons of fixed effects (following omnibus LMM t-test, $t_{20,576} < 2.2$, $p < 0.02$; post-hoc two-sided t-tests, all $p < 0.05$).

Author Manuscript Author Manuscript Author Manuscript Author Manuscript

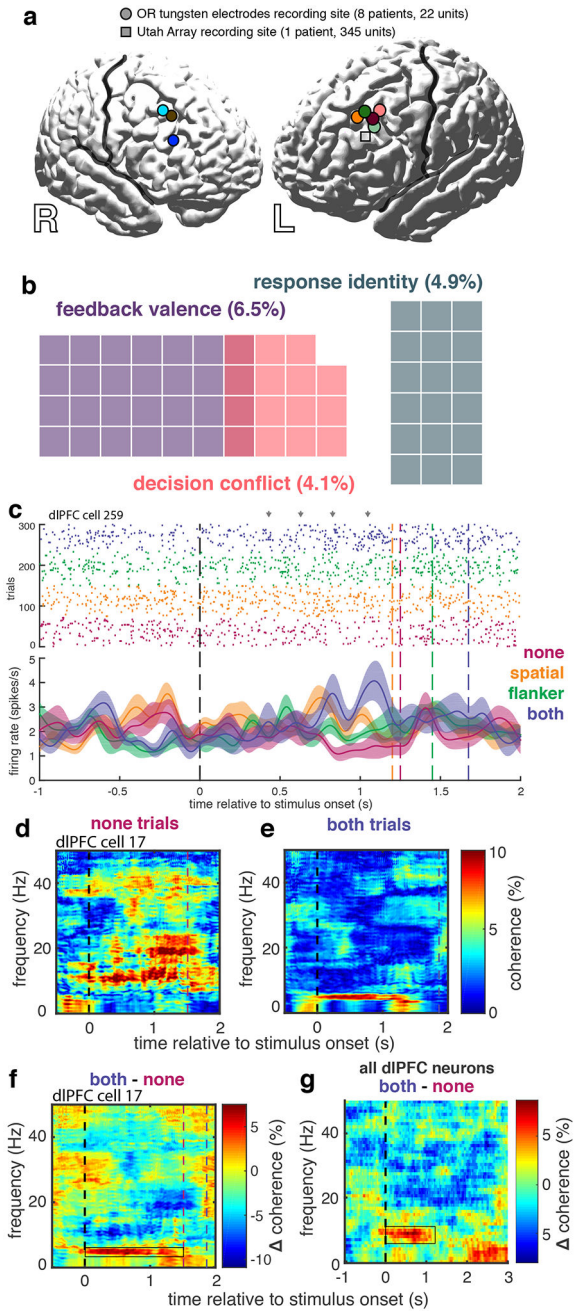

Figure 5. Temporal coding in human dlPFC neurons |

a, Recording locations in the 9 subjects from which dlPFC units were recorded. Circles represent DBS patients and the square represents the epilepsy patient. **b,** Venn diagram showing numbers (and percent, total n = 367) of only those neurons that were selective for specific task features using a rate code. **c,** A representative dlPFC neuron with firing rate coding and temporal (theta) coding (two-sided SFC permutation test, $p < 0.05$) for decision conflict. Conflict conditions are color-coded as in Figure 1. Gray arrows highlight clusters of single unit spikes in a theta-coherent pattern. Shaded regions indicate standard error (n = 58, 86, 88, and 68 trials for none, spatial, flanker, and both conditions, respectively). **d,e,**

Author Manuscript Author Manuscript Author Manuscript Author Manuscript

Representative coherogram for another dlPFC neuron averaged over “none” trials (**d**) and “both” trials (**e**). **f,** Difference coherogram between **d** and **e** illustrating increased coherence between spike timing and theta oscillations (boxed region) in higher conflict trials. **g,** Mean difference coherogram averaged across all 367 dlPFC neurons recorded in all 9 subjects (boxed region shows significant cluster −0.1 to 1.2 s and 4.8 to 10.7 Hz, two-sided SFC permutation tests, all $p < 0.05$). 191 (52.0%) neurons demonstrated spike-theta coupling that scaled with conflict level (LMM t-test, $t_{886} = 4.2$, $p = 3*10^{-5}$).

Author Manuscript Author Manuscript Author Manuscript Author Manuscript

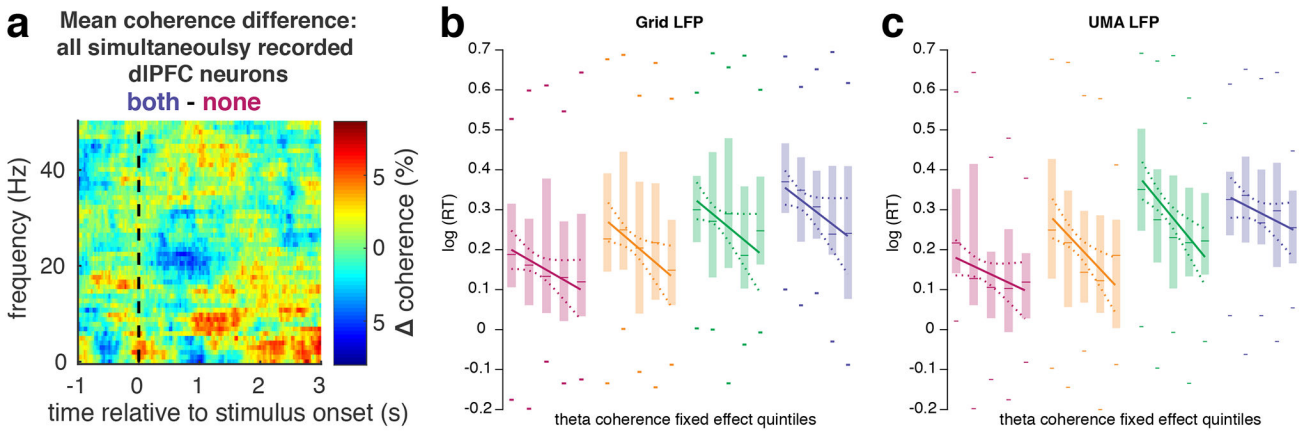

Figure 6. Trial-to-trial encoding of conflict via population theta coherence |

a, Mean difference coherogram averaged across trials (sample sizes listed below) with >100 simultaneously recorded neurons on the dlPFC UMA, illustrating significant difference in coherence across conflict conditions (The cluster of significant coherence was from 0.8 to 1.9 s and 5.4 to 10.7 Hz, two-sided SFC permutation test, all $p < 0.05$). **b,** Box plots (box height: interquartile range, ticks: most extreme points, lines: medians) of theta coherence fixed effect quintiles from the LMM versus log(RT) with overlaid regression lines for each conflict condition, color coded as in Figure 1 (n = 215, 222, 240, and 211 trials for none, spatial, flanker, and both conditions, respectively). **c,** Same as **b,** using down-sampled and filtered data from the UMA for coherence calculations (n = 187, 198, 208, and 176 trials for none, spatial, flanker, and both conditions, respectively).